ILC Damping Rings: Benefit of the Antechamber or: Antechamber vs. SEY*

M. A. Furman,† Center for Beam Physics, LBNL, Berkeley, CA 94720,
and CLASSE, Cornell University, Ithaca, NY 14853

Abstract

We present simulation results of the build-up of the electron-cloud density n_e for the two proposed ILC damping ring lattices, DC04 and DSB3, with particular attention to the potential benefit of an antechamber. We examine a field-free region and a dipole bending magnet, with or without an antechamber. We assume a secondary electron emission model for the chamber surface based on approximate fits to measured data for TiN, except that we let the peak value of the secondary emission yield (SEY), $\delta_{\rm max}$, be a variable. We conclude that there is a critical value of $\delta_{\rm max}$ below which the antechamber provides a substantial benefit, roughly a factor ~ 40 reduction in n_e relative to the case in which $\delta_{\rm max}$ exceeds the critical value. We estimate the steady-state value of n_e as a function of $\delta_{\rm max}$, and thereby obtain the critical value of $\delta_{\rm max}$ for all cases considered. Thus, from the perspective of the electron-cloud effect, the inclusion of an antechamber in the design is justified only if $\delta_{\rm max}$ is below the critical value.

The results presented here constitute a slight extension of those previously presented in March and September, 2010 [1, 2].

INTRODUCTION AND ASSUMPTIONS

The desire to limit the potentially serious adverse consequences from the electron cloud effect (ECE) in the proposed ILC positron damping ring has led to the consideration of adding an antechamber to the vacuum chamber [3], a design decision similar to the one adopted many years ago for the positron ring of the PEP-II collider [4]. The antechamber provides the obvious benefit of extracting from the vacuum chamber a large fraction η (η =antechamber clearing efficiency) of the synchrotron-radiated photons, which are therefore unavaliable to generate photoelectrons.

Fighting against the photon clearing effect of the antechamber is the process of secondary electron emission off the walls of the chamber. The number of secondary electrons grows in time in a compound fashion, and can therefore readily negate the clearing effect of the antechamber. The secondary electron density is a nonlinear function of bunch intensity and of $\delta_{\rm max}$, and exhibits threshold behavior in both of these variables, hence the resulting balance between the antechamber and the SEY of the chamber material is non-trivial.

* Work supported by the US DOE under contract DE-AC02-05CH11231 and by the CESRTA program. Invited talk presented at the ECLOUD10 Workshop (Cornell Univerity, Oct. 8-12, 2010).

† mafurman@lbl.gov

We consider both proposed lattices, DC04 ($C = 6$ km) and DSB3 ($C = 3$ km), and for each of these we examine field-free regions and dipole bending magnets. For each case, we simulate the build-up with and without an antechamber of clearing efficiency $\eta = 98\%$ (Fig. 1). In all cases we set the bunch spacing $t_b = 6$ ns, and then repeat the analysis for most cases for $t_b = 3$ ns. The beam energy and bunch intensity are fixed throughout. The SEY function $\delta(E_0)$ used here is shown in Fig. 2. The emission spectrum corresponds, approximately, to that of TiN, but we let $\delta_{\rm max}$ be an adjustable input parameter on the range $0 - 1.4$. A detailed set of parameters is listed in Tables 1-2.

This being a build-up simulation, the beam is a prescribed (non-dynamical) function of space and time, with bunches of specified sizes, intensity and spacing. The fill pattern simulated consists of 5 trains, as defined in Table 1, whether the bunch spacing is 3 or 6 ns. The electrons, on the other hand, are fully dynamical. The analysis is carried out with the electron-cloud build-up code POSINST [5–8].

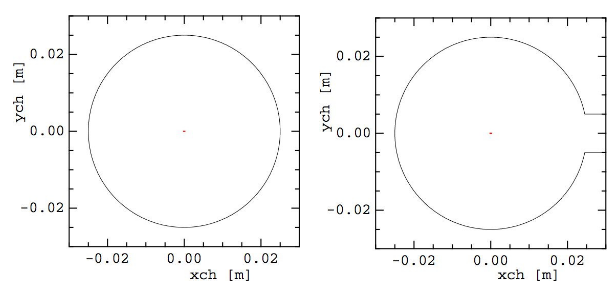

Figure 1: Cross section of the vacuum chamber, without and with an antechamber. The red dot at the center represents the approximate one-sigma beam profile.

RESULTS

Figure 3 shows the build-up of n_e for a field-free section when $t_b = 6$ ns. It is clear that (1) n_e reaches steady state for all values of $\delta_{\rm max}$ examined, (2) the steady-state value is slightly larger for DSB3 than for DC04, and (3) when an antechamber is present, the steady-state value of n_e is a factor ~ 40 lower than the no-antechamber case.

Figure 4 shows the corresponding results for a dipole bending magnet. In this case, one sees that the antechamber also provides a protection factor of ~ 40 only if $\delta_{\rm max}$ is sufficiently low: the critical value of $\delta_{\rm max}$ is ~ 1.2 for DC04, and ~ 1.1 for DSB3. If $\delta_{\rm max}$ exceeds this value, the build-up runs away in time until it reaches the level of the

Table 2: Input parameters that vary from DC04 to DSB3.

	DC04		DSB3	
Circumference [m]	6476.4		3238.2	
Harmonic no.	14042		7021	
n'_γ [photons/e$^+$/m]	0.33		0.47	
n'_e [photo-el./e$^+$/m] (w/o antechamber)	0.033		0.047	
n'_e [photo-el./e$^+$/m] (w. antechamber)	0.66×10^{-3}		0.94×10^{-3}	
	field-free	bend	field-free	bend
Tr. bunch sizes (σ_x, σ_y) [μm]	(360,6)	(260,6)	(270,6)	(110,5)
Dipole field B [T]	0	0.27	0	0.36

Table 1: Assumed global parameters.

Ring and beam	
Beam energy	$E_b = 5$ GeV
Bunch population	$N_b = 2 \times 10^{10}$
RMS bunch length	$\sigma_z = 5$ mm
RF frequency	650 MHz
Bunch train:	
if $t_b = 6.154$ ns: 45 bunches (spacing = 4 buckets)	
$+(15 \times 4 = 60)$ empty buckets	
if $t_b = 3.077$ ns: 45 bunches (spacing = 2 buckets)	
$+(15 \times 2 = 30)$ empty buckets	
Fill pattern simulated	$5 \times$ (train+gap)
Chamber radius	$a = 2.5$ cm
Antechamber full height (if present)	$h = 1$ cm
Antechamber clearing efficiency	$\eta = 98\%$
Quantum efficiency of chamber	QE=0.1
Radiation vertical spot size at wall	$\sigma_y = 1$ mm
Photon reflectivity	$R = 0.9$ *
Peak SEY values explored:	
$\delta_{\max} = 0, 0.9, 1.1, 1.2, 1.3, 1.4$	
Electron energy at $\delta_{\max}$	$E_{\max} = 296$ eV
SEY at $E = 0$	$\delta(0) = 0.31 \times \delta_{\max}$
Simulation parameters	
Primary macroelectrons/bunch	1,000
Max. no. of macroelectrons	20,000
Bunch profile	3D gaussian
Full bunch length	$L_b = 5\sigma_z$
Integration time step Δt:	
during bunch: 1.25×10^{-11} s = 9 kicks/L_b	
outside bunch: $(2.4 - 2.5) \times 10^{-11}$ s	
Space-charge grid	64×64
Grid cell size	$(5 \text{ cm})/64 = 781$ μm

* This implies that, if there is no antechamber, a fraction $1 - R = 0.1$ of the photoelectrons are generated localized at the right "edge" of the chamber. If there is an antechamber, the fraction of the photoelectrons that are generated localized at the right "edge" of the chamber (just above and below the slot) is 5.7×10^{-8}.

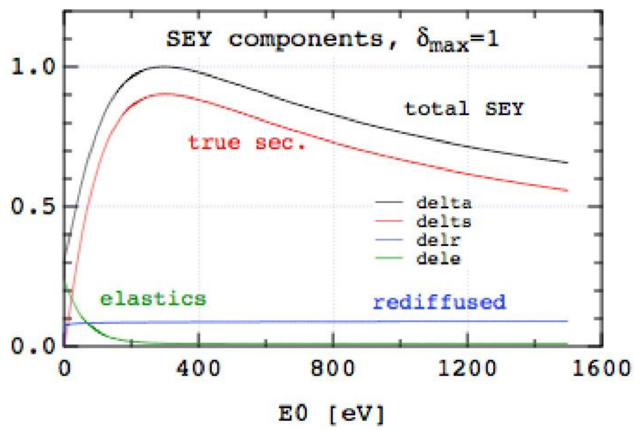

Figure 2: The three main components of the SEY function $\delta(E_0)$, for the case $\delta_{\max} = 1.0$. For other values of $\delta_{\max}$, the three components are scaled by a common factor.

no-antechamber case.[1] In the above-mentioned field-free case, we conclude therefore that the critical value of $\delta_{\max}$ exceeds 1.4, the highest value we exercised. There are simple physical arguments, and plenty of experience in other contexts, that indicates that there is always a critical value of $\delta_{\max}$. Table 3 lists the estimated values of $\delta_{\max}$ for all cases considered in this note.

Figures 5 and 6 compare the build-up for the 3-ns bunch spacing (top plots) with the previously described 6-ns spacing cases (bottom plots), for the DSB3 lattice. One sees the same qualitative features as before, except that the steady-state value of n_e for the 3-ns case is roughly twice that for the 6-ns case.

Tables 4-9 present our results in digitized form for n_e as a function of $\delta_{\max}$. Tables 4-5 summarize the estimated values of the average n_e at saturation, corresponding to the figures above. Tables 6 and 7 show the estimated value of the electron density in the neighborhood of the beam, namely within the 10-σ beam ellipse about the center of the chamber, rather than the overall density. In this case the density is averaged over the bunch length. Finally, Tables

[1] While we have not verified this statement by explicit calculation, we believe it is correct based on basic physical arguments.

Table 3: Critical value of $\delta_{\max}$.

DC04				DSB3			
$t_b = 3$ ns		$t_b = 6$ ns		$t_b = 3$ ns		$t_b = 6$ ns	
field-free	bend	field-free	bend	field-free	bend	field-free	bend
not done	not done	>1.4	~1.2	~1.3	~1.1	>1.4	~1.1

8 and 9 show the estimated electron density also within the 10-σ beam ellipse, except that these values are now the instantaneous values just before the arrival of the bunch at the location being analyzed. These instantaneous 10-σ beam ellipse values of n_e are typically used as inputs to beam dynamics simulations used to study the effects of the electron cloud on the beam (these fall outside the scope of the pressent investigation).

CONCLUSIONS AND DISCUSSION

In general terms, we conclude that:

1. n_e in DSB3 is larger than in DC04 by $10 - 20\%$.
2. The 10-σ front-bunch-density is comparable to the average n_e (within a factor 2 or less).
3. If no antechamber is present:
   (a) n_e has a generally smooth, monotonic dependence on $\delta_{\max}$ in the range examined.
   (b) n_e is $\sim 2\times$ higher for $t_b = 3$ ns than for $t_b = 6$ ns.
4. With antechamber:
   (a) n_e has a 1st-order phase transition as a function of $\delta_{\max}$.
   (b) The critical value of $\delta_{\max}$ is in the range $\sim 1.0-1.3$ (see Table 3), depending on the details of the case examined.
5. If $\delta_{\max}$ is below its critical value, the antechamber reduces n_e by factor ~ 40 relative to no-antechamber case.
6. If $\delta_{\max}$ exceeds its critical value, the antechamber offers no protection.

For the larger values of $\delta_{\max}$ examined, especially if there is no antechamber, the estimated value of n_e is within the range of what is expected to lead to beam instability [3]. For this reason, a more careful assessment might be indicated in order to ascertain with more confidence the regime of the ILC positron damping ring vis-à-vis the ECE.

For example, the sensitivity of our results to the details of secondary emission mode have not been explored here, except for $\delta_{\max}$. It seems desirable to vary $E_{\max}$ by $\pm 20\%$ and see what happens, since this parameter is not precisely known. Ditto for the secondary electron spectrum composition (true secondaries vs. rediffused vs. elastically backscattered electrons). We have also not explored the sensitivity to the antechamber height h, which determines the clearing efficiency η. By exercising both η and $\delta_{\max}$ one would determine the interesting phase diagram $\eta - \delta_{\max}$.

The numerical convergence of our results has been only partly checked. In most cases, we found that 5 trains is sufficiently long for n_e to sensibly reach steady state, provided $\delta_{\max}$ is low enough. A more accurate determination of the critical value of $\delta_{\max}$ for each case would require running the simulation for longer than 5 trains. If we increase the integration time step Δt by a factor of 3, the results do not change much, except for the "runaway cases" pertaining to the bending magnets with antechamber and $\delta_{\max}$ large enough that n_e does not reach steady state by the end of the 5th bunch train. The dependence on the space-charge grid has not been checked, but a 64×64 grid has given quite stable results in other contexts. Ditto for number of macroparticles. The photon reflectivity parameter R has not been exercised, although it is known that high values, such as $R = 0.9$ used in all cases here, tends to yield pessimistic (ie. higher) values for n_e than low values in bending magnets. A fairly accurate value of R might be determined via the program Synrad3D [9]. Finally, we have not assessed the ECE in quads, wigglers, and other regions of the machine. Traditionally, these regions do not contribute significantly to the ECE relative to the bending magnets and field-free regions, although the ILC positron damping ring is probably the first exception to this rule, given the importance of the wigglers.

ACKNOWLEDGMENTS

I am indebted to M. Pivi, M. Palmer and G. Dugan for discussions.

REFERENCES

[1] M. A. Furman, "Status of Ecloud Build-Up Simulations for the ILC DRs," ILC Ecloud Task Force collaboration meeting, 10 March 2010.

[2] M. A. Furman, "Status of Ecloud Build-Up Simulations for the ILC DRs: 3 ns Bunch Spacing," ILC Ecloud Task Force collaboration meeting, 22 September 2010.

[3] M. Pivi, these proceedings.

[4] "PEP-II: An Asymmetric B Factory–Conceptual Design Report," June 1993, LBL-PUB-5379/SLAC-418/CALT-68-1869/UCRL-ID-114055/UC-IIRPA-93-01.

[5] M. A. Furman and G. R. Lambertson, "The electron-cloud instability in the arcs of the PEP-II positron ring," LBNL-41123/CBP Note-246, PEP-II AP Note AP 97.27 (Nov. 25, 1997). Proc. *Intl. Workshop on Multibunch Instabilities in Future Electron and Positron Accelerators "MBI-97"* (KEK, 15-18 July 1997; Y. H. Chin, ed.), KEK Proceedings **97-17**, Dec. 1997, p. 170.

[6] M. A. Furman and M. T. F. Pivi, "Probabilistic model for the simulation of secondary electron emission," LBNL-49771/CBP Note-415 (Nov. 6, 2002). PRST-AB **5** 124404 (2003), http://prst-ab.aps.org/pdf/PRSTAB/v5/i12/e124404.

[7] M. A. Furman and M. T. F. Pivi, "Simulation of secondary electron emission based on a phenomenological probabilistic model," LBNL-52807/SLAC-PUB-9912 (June 2, 2003).

[8] M. A. Furman, "The electron-cloud effect in the arcs of the LHC," LBNL-41482/CBP Note 247/LHC Project Report 180 (May 20, 1998).

[9] G. Dugan, S. Milashuk and D. Sagan, "Synrad3D Photon Propagation and Scattering Simulation," these proceedings.

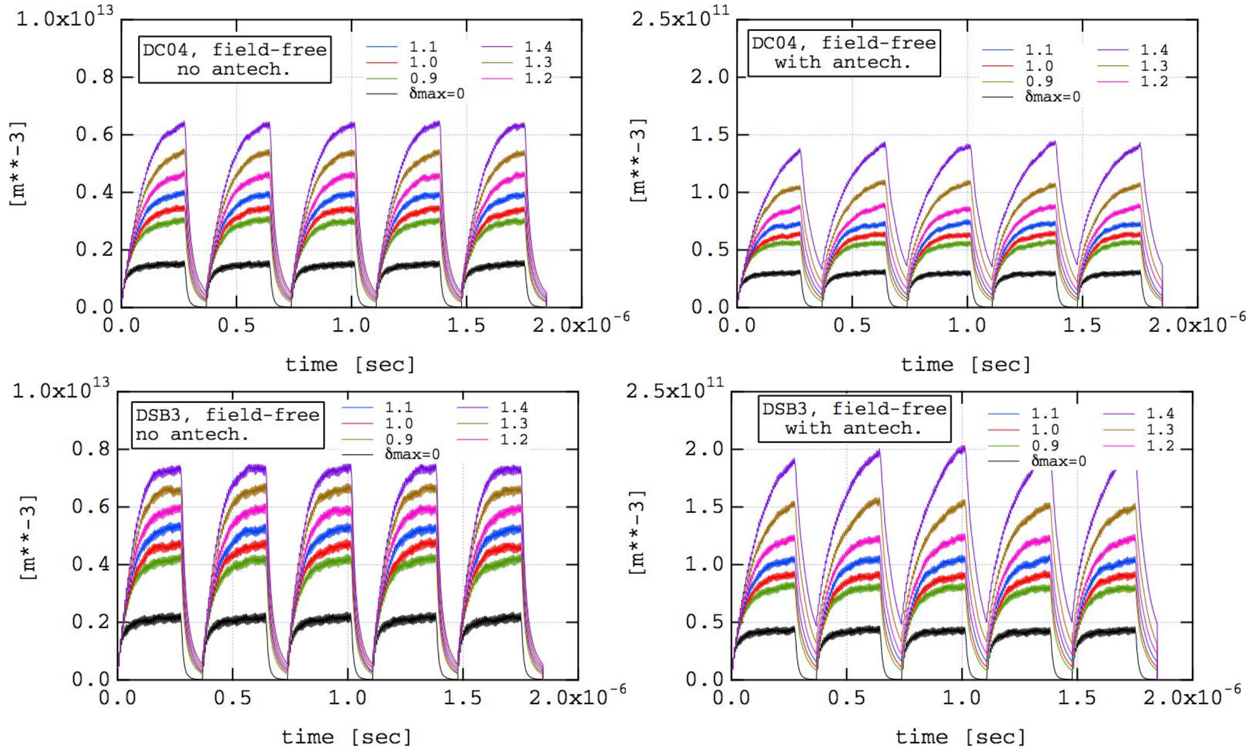

Figure 3: Electron-cloud density averaged over the chamber cross section vs. time for a field-free region and $t_b = 6$ ns. Top: DC04; bottom: DSB3. Note that the vertical scale of the right plots (with antechamber) is a factor 40 lower than in the left ones.

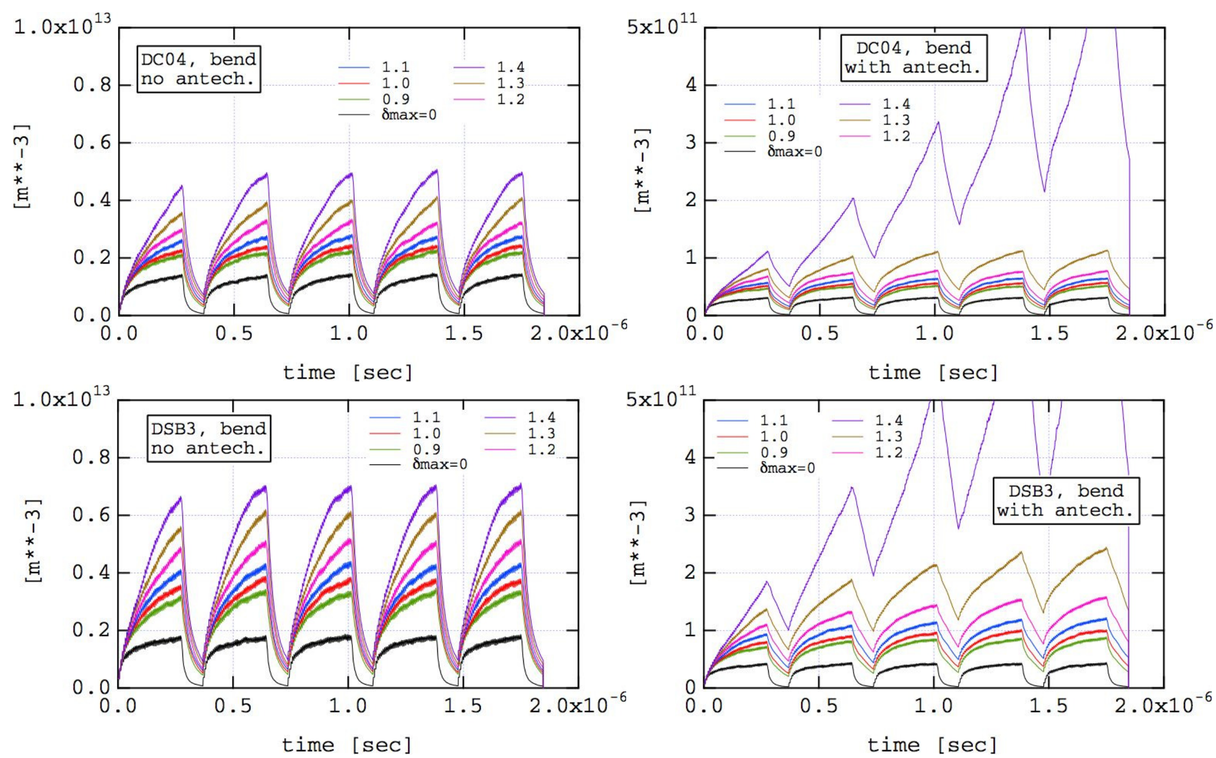

Figure 4: Electron-cloud density averaged over the chamber cross section vs. time for a dipole bending magnet and $t_b = 6$ ns. Top: DC04; bottom: DSB3. Note that the vertical scale of the right plots (with antechamber) is a factor 20 lower than in the left ones.

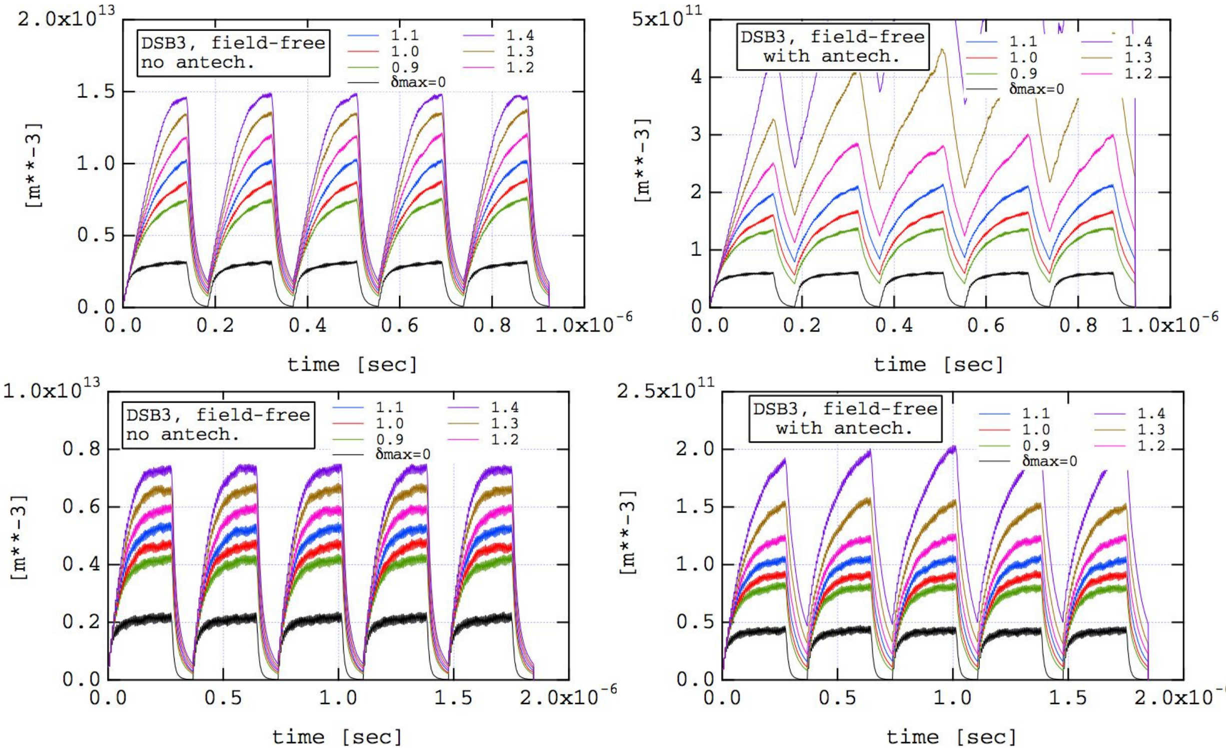

Figure 5: Electron-cloud density averaged over the chamber cross section vs. time for a field-free region for the DSB3 lattice. Top: $t_b = 3$ ns; bottom: $t_b = 6$ ns. Note that the vertical scale of the right plots (with antechamber) is a factor 40 lower than in the left ones.

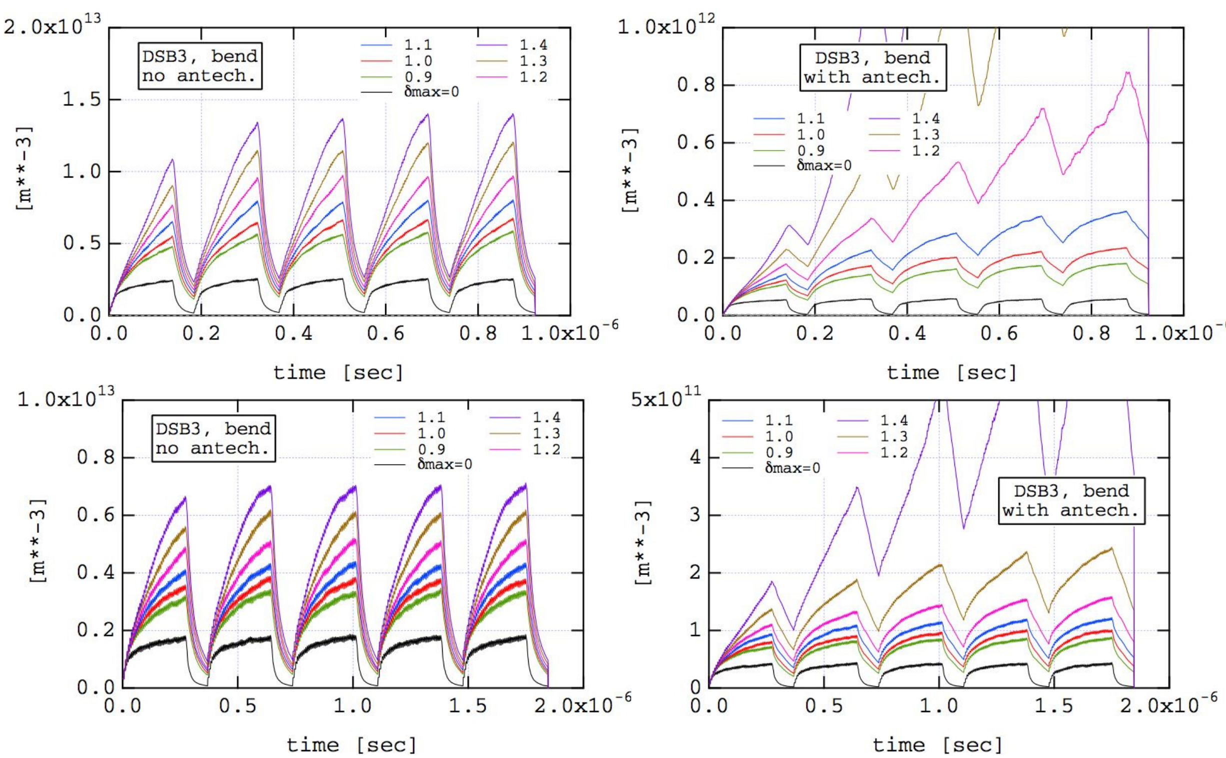

Figure 6: Electron-cloud density averaged over the chamber cross section vs. time for a dipole bending magnet for the DSB3 lattice. Top: $t_b = 3$ ns; bottom: $t_b = 6$ ns. Note that the vertical scale of the right plots (with antechamber) is a factor 20 lower than in the left ones.

Table 4: Overall n_e at saturation* for $t_b = 6$ ns (units: 10^{12} m^{-3})

	DC04				DSB3			
	field-free		bend		field-free		bend	
$\delta_{\max}$	antech.	no antech.	antech.	no antech.	antech.	no antech.	antech.	no antech.
0.0	0.031	1.5	0.032	1.4	0.044	2.2	0.045	1.8
0.9	0.056	3.0	0.054	2.2	0.081	4.3	0.090	3.3
1.0	0.064	3.4	0.058	2.4	0.092	4.6	0.10	3.7
1.1	0.073	3.9	0.065	2.8	0.10	5.3	0.12	4.3
1.2	0.087	4.7	0.079	3.2	0.12	6.0	0.16	5.1
1.3	0.10	5.4	0.11	4.1	0.15	6.6	> 0.2	6.1
1.4	0.14	6.3	> 0.8	5.0	0.20	7.3	> 1	7.0

* Saturation means here "at the end of the last (5th) train of bunches."

Table 5: DSB3: overall n_e at saturation* (units: 10^{12} m^{-3})

	$t_b = 3$ ns				$t_b = 6$ ns			
	field-free		bend		field-free		bend	
$\delta_{\max}$	antech.	no antech.	antech.	no antech.	antech.	no antech.	antech.	no antech.
0.0	0.06	3.2	0.06	2.5	0.044	2.2	0.045	1.8
0.9	0.14	7.7	0.18	5.8	0.081	4.3	0.090	3.3
1.0	0.17	9.0	0.23	6.7	0.092	4.6	0.10	3.7
1.1	0.22	10.1	0.36	7.9	0.10	5.3	0.12	4.3
1.2	0.3	12.1	>0.85	9.6	0.12	6.0	0.16	5.1
1.3	0.5	13.8	>2.75	12	0.15	6.6	>0.2	6.1
1.4	>1.2	15	>5	14	0.20	7.3	>1	7.0

* Saturation means here "at the end of the last (5th) train of bunches."

Table 6: n_e within 10 beam σ's at saturation,* averaged over bunch length, for $t_b = 6$ ns (units: 10^{12} m^{-3})

	DC04				DSB3			
	field-free		bend		field-free		bend	
$\delta_{\max}$	antech.	no antech.	antech.	no antech.	antech.	no antech.	antech.	no antech.
0.0	0.08	5.0	0.01	0.6	0.12	9	0.015	0.7
0.9	0.18	10	0.035	1.6	0.22	14	0.03	1.5
1.0	0.20	11	0.046	1.6	0.26	14	0.04	2.0
1.1	0.22	14	0.065	3.1	0.31	19	0.09	2.3
1.2	0.25	15	0.11	4.5	0.41	20	0.05	3.0
1.3	0.35	16	0.25	6.0	0.48	23	0.2	3.5
1.4	0.44	20	>4	8.0	0.62	24	>0.6	4.5

* Saturation means here "at the end of the last (5th) train of bunches." These data have large statistical errors, $\sim 50\%$ or more.

Table 7: DSB3: n_e within 10 beam σ's at saturation* (units: 10^{12} m^{-3})

	$t_b = 3$ ns				$t_b = 6$ ns			
	field-free		bend		field-free		bend	
δ_{max}	antech.	no antech.	antech.	no antech.	antech.	no antech.	antech.	no antech.
0.0	0.2	10	0.02	0.8	0.12	9	0.015	0.7
0.9	0.5	25	0.06	2	0.22	14	0.03	1.5
1.0	0.5	28	0.07	2.2	0.26	14	0.04	2.0
1.1	0.7	30	0.12	3	0.31	19	0.09	2.3
1.2	0.75	30	0.2	3.5	0.41	20	0.05	3.0
1.3	>1.4	35	>0.3	4	0.48	23	0.2	3.5
1.4	>3	40	>0.3	5	0.62	24	>0.6	4.5

* Saturation means here "at the end of the last (5th) train of bunches." These data have large statistical errors, $\sim 50\%$ or more.

Table 8: n_e at bunch front within 10 beam σ's for $t_b = 6$ ns* (units: 10^{12} m^{-3})

	DC04				DSB3			
	field-free		bend		field-free		bend	
δ_{max}	antech.	no antech.	antech.	no antech.	antech.	no antech.	antech.	no antech.
0.0	0.024	1.2	0.023	1.0	0.034	1.7	0.031	1.3
0.9	0.044	2.3	0.038	1.6	0.063	3.2	0.063	2.4
1.0	0.050	2.6	0.042	1.8	0.070	3.6	0.073	2.6
1.1	0.057	3.0	0.048	1.9	0.081	4.0	0.086	2.9
1.2	0.066	3.4	0.056	2.2	0.94	4.5	0.10	3.4
1.3	0.080	3.9	0.079	2.6	0.11	5.0	>0.2	3.9
1.4	0.10	4.5	>0.3	3.1	0.14	5.6	>0.3	4.6

* These data have large statistical errors, $\sim 50\%$ or more. Within these errors, there is no difference between the time-averaged density and the instantaneous density at the last bunch in the train.

Table 9: DSB3: n_e at bunch front within 10 beam σ's (units: 10^{12} m^{-3})

	$t_b = 3$ ns				$t_b = 6$ ns			
	field-free		bend		field-free		bend	
δ_{max}	antech.	no antech.	antech.	no antech.	antech.	no antech.	antech.	no antech.
0.0	0.1	5	0.02	0.6	0.034	1.7	0.031	1.3
0.9	0.25	10	0.04	1.6	0.063	3.2	0.063	2.4
1.0	0.28	11	0.05	2.3	0.070	3.6	0.073	2.6
1.1	0.35	13	0.1	1.9	0.081	4.0	0.086	2.9
1.2	0.45	15	0.12	3.0	0.94	4.5	0.10	3.4
1.3	0.64	16	0.23	3.3	0.11	5.0	>0.2	3.9
1.4	>1.2	16	>0.7	4.4	0.14	5.6	>0.3	4.6

* These data have large statistical errors, $\sim 50\%$ or more. Within these errors, there is no difference between the time-averaged density and the instantaneous density at the last bunch in the train.